

submitted to *The Astrophysical Journal*

Are Silicon Nanoparticles an Interstellar Dust Component?

Aigen Li and B.T. Draine

Princeton University Observatory, Peyton Hall, Princeton, NJ 08544, USA;
agli@astro.princeton.edu, draine@astro.princeton.edu

ABSTRACT

Silicon nanoparticles have been proposed as the source of the observed “extended red emission” (ERE) from interstellar dust. We calculate the thermal emission expected from such particles in a reflection nebula such as NGC 2023. Pure Si nanoparticles would emit at $16.4\mu\text{m}$, while Si core-SiO₂ mantle nanoparticles produce a feature at $21\mu\text{m}$.

The observed ERE intensity and upper limits on the 16.4 and $21\mu\text{m}$ features toward NGC 2023 give a lower limit on the required photoluminescence efficiency η_{PL} . With current uncertainties in the foreground extinction $1.2 \lesssim A_{0.68\mu\text{m}} \lesssim 3.2$ to NGC 2023, we find $\eta_{\text{PL}} > 17\%$ for pure Si nanoparticles, or $\eta_{\text{PL}} > 33\%$ for Si core-SiO₂ mantle nanoparticles. Measurement of the R band extinction toward the ERE-emitting region would allow these lower limits to be made stronger.

Subject headings: dust, extinction — infrared: ISM: lines and bands — reflection nebulae: NGC 2023

1. Introduction

First detected in the Red Rectangle (Schmidt, Cohen, & Margon 1980), “extended red emission” (ERE) from interstellar dust consists of a broad, featureless emission band between $\sim 5400\text{\AA}$ and 9000\AA , peaking at $6100 \lesssim \lambda_p \lesssim 8200\text{\AA}$, and with a width $600\text{\AA} \lesssim \text{FWHM} \lesssim 1000\text{\AA}$. The ERE has been seen in a wide variety of dusty environments, ranging from the diffuse interstellar medium of our Galaxy, reflection nebulae, planetary nebulae, HII regions, to other galaxies (see Witt, Gordon, & Furton 1998 for a summary). The ERE is generally attributed to photoluminescence (PL) by some component of interstellar grains, powered by ultraviolet (UV)/visible photons. The photon conversion efficiency in the diffuse interstellar medium has been determined to be near $(10 \pm 3)\%$ (Gordon et al. 1998; Szomoru & Guhathakurta 1998) assuming that 1) all UV/visible photons absorbed by interstellar grains are absorbed by the ERE carrier; and 2) the absorption of one UV/visible photon leads to one ERE photon. This implies that the actual PL photon conversion efficiency of the ERE carrier must substantially exceed $\sim 10\%$ since the ERE carrier is unlikely to be the only UV/visible photon absorber.

Various forms of carbonaceous materials – hydrogenated amorphous carbon (HAC) (Duley 1985; Witt & Schild 1988), polycyclic aromatic hydrocarbons (PAHs) (d'Hendecourt et al. 1986), quenched carbonaceous composite (QCC) (Sakata et al. 1992), C₆₀ (Webster 1993), coal (Papoulier et al. 1996), PAH clusters (Allamandola, private communication), and carbon nanoparticles (Seahra & Duley 1999) – have been proposed as carriers of ERE. However, most of them appear to be unable to simultaneously match the observed ERE spectra and the required PL efficiency (see Witt et al. 1998 for details)¹. Very recently, Witt et al. (1998) and Ledoux et al. (1998) suggested crystalline silicon nanoparticles (SNPs) with 15Å – 50Å diameters as the carrier on the basis of experimental data showing that SNPs could provide a close match to the observed ERE spectra and satisfy the quantum efficiency requirement. It was estimated by Witt et al. (1998) and Ledoux et al. (1998) that SNPs account for $\lesssim 5\%$ of the total interstellar dust mass and ≈ 6 Si per 10^6 H atoms. Zubko et al. (1999) modelled the interstellar extinction curve taking SNPs as an interstellar dust component containing ≈ 18 Si per 10^6 H atoms, or $\sim 50\%$ of solar Si abundance.

Although pure silicon crystals have only weak infrared bands resulting from multiphonon processes, these emission features may be observable because of the required large quantity of SNPs (see previous paragraph) whenever starlight intensities are high enough to heat these particles to $T \gtrsim 50$ K. On the other hand, as discussed in Witt et al. (1998), SNPs are very likely coated by a SiO₂ shell, in which case one might expect to see 9.1 and 21μm Si-O vibrational modes if SNPs are indeed an interstellar dust component.

The purpose of this *Letter* is to test the SNP hypothesis by calculating the IR spectra for SNPs in a reflection nebula – NGC 2023 – and comparing with observations. We consider NGC 2023 rather than the diffuse interstellar medium of our Galaxy (the so-called “IR cirrus”) because: (1) Witt & Boroson (1990) have measured the ERE in NGC 2023, finding it to be consistent with the PL spectra of 36.5Å diameter Si nanocrystals (Ledoux et al. 1998); (2) The dust in NGC 2023 is heated (by absorption of starlight) to temperatures high enough to radiate in infrared modes at 16 and 21μm, whereas in the diffuse ISM only the very small ($a \lesssim 10$ Å) grains reach temperatures $\gtrsim 100$ K required for emission at these wavelengths; (3) Verstraete et al. (2001) have obtained the 2.4–45μm spectrum of NGC 2023 using the *Infrared Space Observatory* (ISO).

In §2 we discuss the optical properties of silicon nano-crystals and glassy SiO₂ (§2.1) as well as the heat capacities of pure silicon and silicon core-SiO₂ mantle grains (§2.2). In §3 we carry out calculations for the IR emission spectra of SNPs (with or without SiO₂ coatings), and discuss their implications. In §4 we discuss the effects of grain shape, mantle thickness, and sources of uncertainties. Our conclusions are presented in §5.

¹Seahra & Duley (1999) argued that small carbon clusters were able to meet both the ERE profile and the PL efficiency requirements. However, this hypothesis is ruled out by non-detection in NGC 7023 of the 1μm ERE peak (Gordon et al. 2000) predicted by the carbon nanoparticle model.

2. Grain Physics

2.1. Optical Properties

Due to the lack of knowledge of the optical properties for silicon nanoparticles over a wide wavelength range, we apply the following “synthetic” procedure to obtain the complex indices of refraction $m(\lambda) = m' + im''$. For $0.055 < \lambda < 0.85\mu\text{m}$ we adopt the imaginary part m'' for Si nanocrystals (Koshida et al. 1993); for $0.001 < \lambda < 0.055\mu\text{m}$ we take m'' for bulk crystalline Si (Adachi 1999); for $1.0 < \lambda < 3.6\mu\text{m}$ we set $m'' = 2.4 \times 10^{-8}$ estimated from the (room temperature) absorption coefficient $\alpha \approx 10^{-3} \text{ cm}^{-1}$ of bulk Si between 1 and $3\mu\text{m}$ (Gray 1972). For the IR range, since there are no measurements made for Si nanoparticles, we adopt those of bulk Si: for $3.6 < \lambda < 25\mu\text{m}$ we take those of Palik (1985) for crystalline bulk silicon; extrapolation is then made for $\lambda > 25\mu\text{m}$.² After smoothly joining the adopted m'' , we calculate m' from m'' through the Kramers-Kronig relation (Bohren & Huffman 1983, p. 28). In Figure 1 we plot the “synthesized” optical constants for crystalline SNPs. For comparison, the optical constants for bulk crystalline silicon (Palik 1985; Adachi 1999) are also plotted. As noted by Zubko et al. (1999), the UV/visual optical properties for SNPs differ considerably from those of bulk silicon.³

For glassy SiO_2 , we take m'' from Palik (1985) but with two modifications: 1) for $0.15 < \lambda < 3.6\mu\text{m}$ we set $m'' = 1.0 \times 10^{-4}$ based on the absorption coefficient measured by Harrington et al. (1978); 2) for $\lambda > 160\mu\text{m}$, we extrapolate m'' from the values for $\lambda < 160\mu\text{m}$. Again, the real part m' is calculated from the Kramers-Kronig relation. The results are also presented in Figure 1.

2.2. Enthalpies

The experimental specific heat of bulk crystalline silicon can be approximated by a Debye model (with dimensionality $n = 3$) and Debye temperature $\Theta = 530 \text{ K}$, while SiO_2 glass can be approximated by a model where 1/3 of the vibrational modes are distributed according to a Debye model with $\Theta = 275 \text{ K}$, and 2/3 of the modes according to a Debye model with $\Theta = 1200 \text{ K}$.

For very small particles at low temperatures, the discrete nature of the vibrational spectrum

²We do not adopt those of Palik (1985) for $\lambda > 25\mu\text{m}$ since they were measured at room temperature; the long-wavelength absorptivity of Si nanocrystals at low temperatures is expected to be much lower due to the reduced conductivity. But we have also tried the room temperature emissivity by adopting the m'' of Palik (1985) for $3.6 < \lambda < 300\mu\text{m}$, and deriving m'' from the room temperature absorption coefficient (Gray 1972) for $300 < \lambda < 1000\mu\text{m}$. For pure Si grains in the NGC 2023 radiation field discussed below, the $16.4\mu\text{m}$ emission feature is only reduced by $\sim 10\%$. For Si core- SiO_2 mantle grains, the far-IR emissivity of the Si core is unimportant since the thermal emission is dominated by the SiO_2 mantle. Thus our conclusions do not depend on the choice of m'' for Si in the far-IR.

³The IR bands of Si nanoparticles may become stronger due to the symmetry-breaking surfaces (e.g., see Hofmeister, Rosen, & Speck 2000). New IR bands, forbidden in bulk silicon, may also appear (Adachi, private communication). Unfortunately, IR measurements of Si nanoparticles are unavailable, so we must use the optical properties of bulk Si.

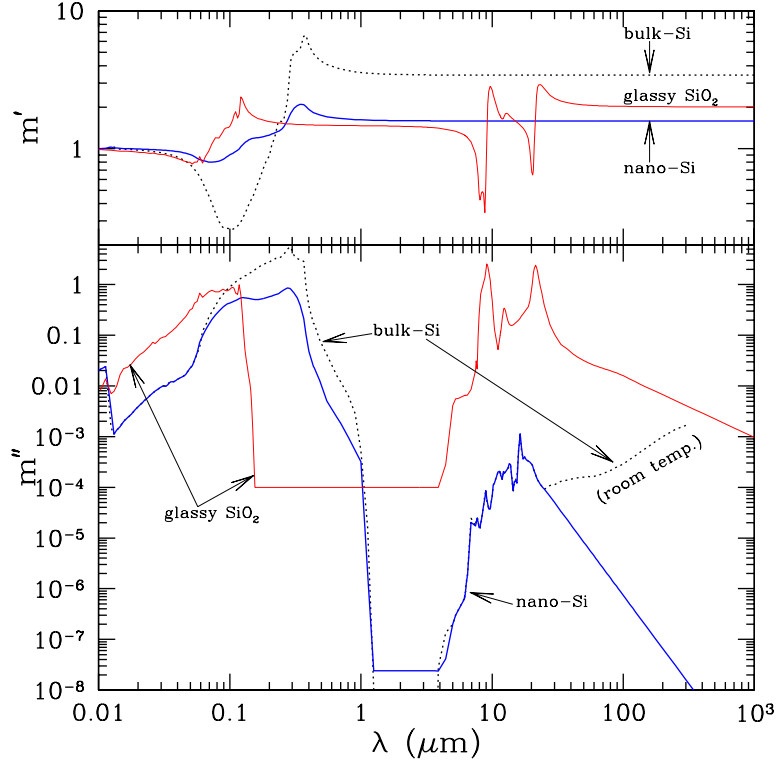


Fig. 1.— Optical constants m' (upper panel), m'' (lower panel) of crystalline nano-silicon (heavy lines) and SiO_2 glass (thin lines). Also plotted are those of bulk silicon (dotted lines).

becomes important. Let $N_{\text{atom}}^{\text{Si}}$ and $N_{\text{atom}}^{\text{SiO}_2}$ be the number of atoms in the Si core and SiO_2 mantle, and $N_{\text{atom}} \equiv N_{\text{atom}}^{\text{Si}} + N_{\text{atom}}^{\text{SiO}_2}$ be the total number of atoms. For pure Si clusters, we set $N_m = 3N_{\text{atom}}^{\text{Si}} - 6$ vibrational modes where the “-6” term allows for the translational and rotational degrees of freedom since the energy from photon absorption is only distributed among the vibrational modes. For Si/ SiO_2 nanoparticles, we assume $N_m = 3N_{\text{atom}}^{\text{Si}} - 3$ modes distributed according to a $\Theta = 530$ K Debye model, $N_m = 2N_{\text{atom}}^{\text{SiO}_2} - 2$ modes distributed according to a $\Theta = 1200$ K Debye model, and $N_m = N_{\text{atom}}^{\text{SiO}_2} - 1$ modes distributed according to a $\Theta = 275$ K Debye model. We assume the mode frequencies to be distributed following eqs.(4-6) and eq.(11) of Draine & Li (2001). The specific heat is calculated treating the modes as harmonic oscillators, with the continuum limit used for large particles and high energies (see Draine & Li 2001).

3. IR Emission Spectrum and Its Implications

Let Z_{Si} be the amount of silicon in the grains (by number) relative to total hydrogen. The IR emissivity per unit solid angle per H nucleon from the silicon nanoparticles is

$$j_{\lambda}(a) = \frac{Z_{\text{Si}}}{N_{\text{Si}}(a)} C_{\text{abs}}(a, \lambda) \int_0^{\infty} dT B_{\lambda}(T) P(a, T) \quad (1)$$

where $N_{\text{Si}}(a)$ is the number of Si atoms in a grain of radius a [$N_{\text{Si}} = (\pi a^3/21m_{\text{H}})\rho_{\text{Si}}$ for pure Si nanoparticles, and $N_{\text{Si}} = \pi a_{\text{Si}}^3 \rho_{\text{Si}}/21m_{\text{H}} + \pi(a^3 - a_{\text{Si}}^3)\rho_{\text{SiO}_2}/45m_{\text{H}}$ for grains with Si cores of radius a_{Si} and SiO_2 mantles, where ρ_{Si} , ρ_{SiO_2} are the mass densities of crystalline silicon material ($\approx 2.42 \text{ g cm}^{-3}$) and glassy SiO_2 ($\approx 2.2 \text{ g cm}^{-3}$), respectively, and m_{H} is the mass of a hydrogen atom]; $C_{\text{abs}}(a, \lambda)$ is the absorption cross section of the core-mantle grain of size a at wavelength λ , calculated from Mie theory using the optical constants synthesized in §2.1; $B_{\lambda}(T)$ is the Planck function; $P(a, T)dT$ is the probability that the grain vibrational temperature will be in $[T, T + dT]$. For a given radiation field, we calculate $P(a, T)$ for small grains employing the “*thermal-discrete*” method described in Draine & Li (2001).⁴ We characterize the intensity of the illuminating starlight by χ , the intensity at 1000 Å relative to the Habing (1968) radiation field, with the spectrum assumed to be that of a blackbody of temperature T_{eff} , cutoff at the Lyman edge.

3.1. NGC 2023

The reflection nebula NGC 2023, at a distance $D = 450 \text{ pc}$, is illuminated by the B1.5V star HD 37903 ($T_{\text{eff}} = 22,000 \text{ K}$, $L_{\star} = 7600L_{\odot}$). A modest HII region surrounds the star, beyond which is a photodissociation region at an estimated distance $\sim 5 \times 10^{17} \text{ cm}$ from the star. The radiation field is expected to have an intensity $\chi \approx 5000$ at this distance from the star. While $\chi \approx 5000$ is consistent with models to reproduce the observed IR and far-red emission from UV-pumped H_2 in the bright “emission bar” 80'' S of HD 37903 (Draine & Bertoldi 1996, 2000), the integrated infrared 5–60 μm surface brightness at a position 60'' S of HD 37903 (Figure 3) points to a lower value of χ . We will assume that the dust producing the measured infrared spectrum and ERE is illuminated by a radiation field with $\chi \approx 2000$.⁵

Witt & Boroson (1990) reported ERE measurements with a 7.8'' \times 10.5'' aperture at positions 15'' and 30'' N of HD 37903. The 2.4–45 μm spectrum has been obtained by Verstraete et al. (2001) using the Infrared Space Observatory, using apertures ranging from 14'' \times 20'' (for 2.4–12 μm) to 20'' \times 33'' (for 29–45 μm), at a position 60'' S of HD 37903. Far-infrared photometry with a 37'' beam centered 60'' S of HD 37903 has been obtained from the Kuiper Airborne Observatory by Harvey et al. (1980).

The PDR in NGC 2023 is optically thick to the illuminating starlight. Allowing for forward scattering, we estimate that the effective attenuation cross section per H nucleon for 3–11 eV photons is $\sim 0.5 \times 10^{-21} \text{ cm}^2 \text{ H}^{-1}$, and we approximate the PDR as a slab of optically-thin dust and gas with $N_{\text{H}} \approx 2 \times 10^{21} \text{ cm}^{-2}$. We further assume a limb-brightening factor $1/\cos \theta \approx 2$, where

⁴To be precise, the energy released in the form of PL (ERE photons, with mean energy $\langle h\nu \rangle_{\text{ERE}} \approx 1.8 \text{ eV}$) is not available as heat. The fraction of absorbed photon energy lost to photoluminescence $\eta_{\text{PL}} \langle h\nu \rangle_{\text{ERE}} / \langle h\nu \rangle_{\text{abs}}$ is only 0.24 η_{PL} for pure Si ($\langle h\nu \rangle_{\text{abs}} = 7.5 \text{ eV}$) or 0.20 η_{PL} for SiO_2 -coated Si ($\langle h\nu \rangle_{\text{abs}} = 8.8 \text{ eV}$). Even for $\eta_{\text{PL}} \rightarrow 1$, this is a minor correction which does not alter our conclusions.

⁵As explained in §4, our analysis is insensitive to the precise value assumed for χ .

θ is the angle between the slab normal and our line-of-sight (we note that our final results are insensitive to the adopted values of N_{H} and $1/\cos\theta$; see §4). With the above assumptions, j_{λ} , the power radiated per H nucleon per unit solid angle per unit wavelength λ (see eq.[1]) is related to the observed intensity I_{λ} by

$$I_{\lambda} = \frac{N_{\text{H}}}{\cos\theta} j_{\lambda} 10^{-0.4A_{\lambda}} \approx 4 \times 10^{21} \text{ cm}^{-2} j_{\lambda} 10^{-0.4A_{\lambda}} \quad (2)$$

where A_{λ} is the extinction between the point of emission and the observer.

The foreground extinction A_{λ} is uncertain. The line-of-sight to HD 37903 has $E(B-V) \approx 0.35$ and $R_V \equiv A_V/E(B-V) = 4.1$ (Cardelli, Clayton, & Mathis 1989), corresponding to $A_{0.68\mu\text{m}} \approx 1.2$. For the emission bar $80''$ S of HD 37903, an extinction $A_{2.2\mu\text{m}} \approx 0.5$ has been determined from the relative strengths of H₂ emission lines (Draine & Bertoldi 2000); for an $R_V = 4.1$ (Cardelli et al. 1989) extinction law, this would correspond to $A_{0.68\mu\text{m}} \approx 6.4 A_{2.2\mu\text{m}} \approx 3.2$. Optical images of NGC 2023 (e.g., Witt & Malin 1989) suggest that the surface brightness $30''$ N may be somewhat lower than to the south of HD 37903, so the foreground extinction there might perhaps exceed that for the southern emission bar. For purposes of discussion, we will assume that the extinction to the reflection region $30''$ N of HD37903 (where the ERE has been measured) is likely to be in the range $1.2 \lesssim A_{0.68\mu\text{m}} \lesssim 3.2$.

The *observed* ERE intensity $30''$ N of HD37903 is $\int I_{\lambda}^{\text{ERE}} d\lambda \approx 1.4 \times 10^{-4} \text{ erg cm}^{-2} \text{ s}^{-1} \text{ sr}^{-1}$ (Witt & Boroson 1990), so the ERE emissivity per H nucleon is

$$\int j_{\lambda}^{\text{ERE}} d\lambda = \frac{\int I_{\lambda}^{\text{ERE}} 10^{0.4A_{\lambda}} d\lambda}{N_{\text{H}}/\cos\theta} \approx 3.50 \times 10^{-26} 10^{0.4A_{0.68\mu\text{m}}} \text{ erg s}^{-1} \text{ sr}^{-1} \text{ H}^{-1} \quad (3)$$

Proposed ERE carriers must provide this level of emission.

In Figure 3 we plot the infrared spectrum at a location $60''$ S of HD 37903. Proposed ERE carriers must not exceed the observed IR emission.

3.2. Pure Silicon Grains

We first calculate the IR emission spectra for *pure* crystalline silicon grains illuminated by radiation from HD 37903 with intensity $\chi = 2000$. As shown in Figure 2, the radiation field is so strong that grains with $a \gtrsim 20\text{\AA}$ attain a steady-state temperature $\approx 300\text{K}$ ($\approx 73\text{K}$ for SiO₂-coated grains [see §3.3]; the single-photon heating effect [Greenberg 1968] is evident for $a_{\text{Si}} = 10\text{\AA}$). In Figure 3a we present the predicted spectra for $Z_{\text{Si}} = 3\text{ppm}$ in Si nanoparticles⁶ with radii $a = 10, 20, 30, 40, 50\text{\AA}$. Grains with $a \lesssim 100\text{\AA}$ are in the Rayleigh limit through the whole wavelength range of interest ($\lambda > 912\text{\AA}$) and thus their “equilibrium” temperatures are independent of a ;

⁶Corresponding to the Si/H=3 $\times 10^{-6}$ in Si *cores* which Witt et al. (1998) proposed to explain the observed ERE intensity of the diffuse interstellar medium.

therefore, for a given nanoparticle abundance Z_{Si} , the resulting IR intensity is almost independent of grain size [see eq.(1) where $P(a, T)$ is a δ function].

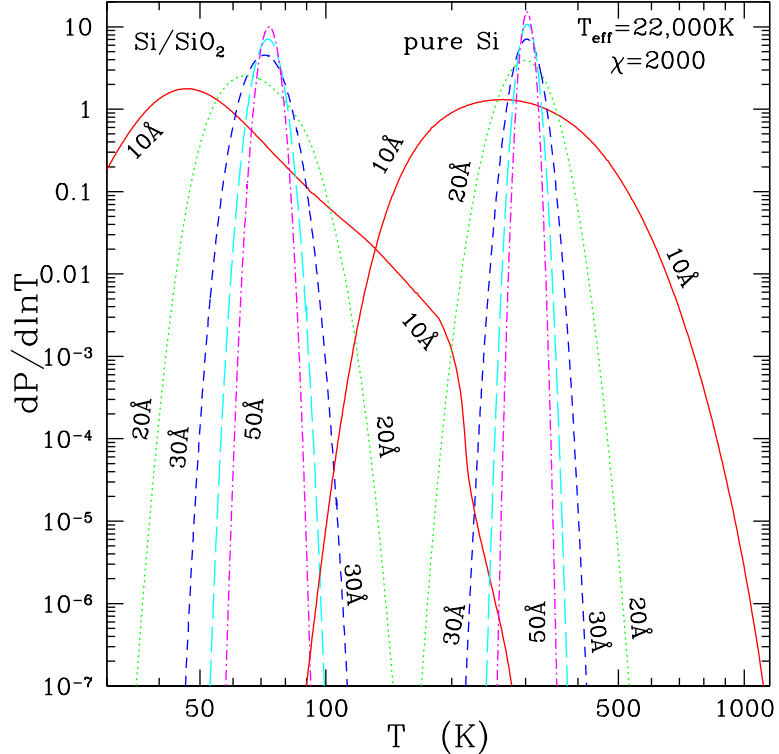


Fig. 2.— Temperature distribution functions for pure silicon grains (right) of radius 10 \AA (solid), 20 \AA (dotted), 30 \AA (short dashed), 40 \AA (long dashed), 50 \AA (dot-dashed); and Si/SiO₂ grains (left) with silicon *core* radius $a_{\text{Si}} = 10\text{\AA}$ (solid), 20 \AA (dotted), 30 \AA (short dashed), 40 \AA (long dashed), 50 \AA (dot-dashed). These grains are illuminated by a starlight intensity of $T_{\text{eff}} = 22,000\text{ K}$ and $\chi = 2000$.

Although the fundamental lattice vibration of crystalline Si has no dipole moment and thus is IR inactive (i.e., there is no interaction between a single phonon and IR radiation), multi-phonon processes produce prominent bands at 6.91, 7.03, 7.68, 8.9, 11.2, 13.5, 14.5, 16.4, and 17.9 μm (Johnson 1959). As seen in Figure 3a, the 16.4 μm emission feature is calculated to be about 3 times stronger than the observational data. In order not to exceed the observed spectrum near 16 μm , $Z_{\text{Si}} \lesssim 1\text{ ppm}$.

Let η_{PL} be the photon conversion efficiency, γ_{Si} be the UV/visual photon absorption rate (in the 912–5500 \AA wavelength range), $\langle h\nu \rangle_{\text{abs}}$ be the mean absorbed photon energy, and $\langle h\nu \rangle_{\text{ERE}}$ be the mean energy of ERE photons. Since the NGC 2023 ERE peaks at $\sim 6800\text{\AA}$ (Witt & Boroson 1990), we take $\langle h\nu \rangle_{\text{ERE}} \approx 1.8\text{ eV}$. Illuminated by starlight of $T_{\text{eff}} = 22,000\text{ K}$, Si nanoparticles are estimated to have $\gamma_{\text{Si}} \approx 2.79 \times 10^{-6} (\chi/2000) \text{ s}^{-1} \text{ Si}^{-1}$ and $\langle h\nu \rangle_{\text{abs}} \approx 7.5\text{ eV}$. The ERE emissivity per H is then $\int j_{\lambda}^{\text{ERE}} d\lambda = \langle h\nu \rangle_{\text{ERE}} \gamma_{\text{Si}} \eta_{\text{PL}} Z_{\text{Si}} / 4\pi \approx 6.40 \times 10^{-19} \eta_{\text{PL}} Z_{\text{Si}} \text{ erg s}^{-1} \text{ sr}^{-1} \text{ H}^{-1}$. From eq. (3) we thus require $\eta_{\text{PL}} Z_{\text{Si}} \approx 5.47 \times 10^{-8} 10^{0.4 A_{0.68\mu\text{m}}}$.

Since we have seen that $Z_{\text{Si}} \lesssim 1\text{ppm}$, it follows that pure Si nanoparticles could produce the observed ERE only if the photoluminescence efficiency $\eta_{\text{PL}} \gtrsim 0.055 \times 10^{0.4A_{0.68\mu\text{m}}}$.

3.3. Silicon Core- SiO_2 Mantle Grains

It seems unlikely that *pure* Si nanoparticles would exist in interstellar space without some degree of oxidation. Experiments show that Si nanocrystals in air spontaneously form an overlayer of SiO_2 which is usually $\sim 10\text{\AA}$ thick (Ledoux et al. 1998). Witt et al. (1998) propose that silicon nanoparticles in the form of Si core- SiO_2 mantle structure are a product of the initial dust formation process through the nucleation of SiO in oxygen-rich stellar mass outflows.

We now calculate the IR emission spectra for Si core- SiO_2 mantle particles. Following Witt et al. (1998), we assume equal numbers of Si atoms in the core and in the mantle – i.e., a core radius $a_{\text{Si}} = (1 + 15\rho_{\text{Si}}/7\rho_{\text{SiO}_2})^{-1/3} a \approx 0.668a$. In Figure 3b we show the theoretical spectra for $a_{\text{Si}} = 10, 20, 30, 40, 50\text{\AA}$ with $Z_{\text{Si}} = 6\text{ppm}$ (estimated by Witt et al. [1998] for Si/SiO_2 grains to account for the ERE in the diffuse ISM). As illustrated in Figure 3b the Si-O modes produce strong features at $21\mu\text{m}$ (transverse vibration), $12.5\mu\text{m}$ (symmetric pumping vibration), and $9.1\mu\text{m}$ (asymmetric valency vibration). The most conspicuous feature is the strong and broad $21\mu\text{m}$ band which is about 8 times stronger than the observational data. To depress the $21\mu\text{m}$ emission feature to the level not in contradiction with the observational spectrum, the silicon depletion $Z_{\text{Si}} \lesssim 0.75\text{ppm}$.

The $912\text{--}5500\text{\AA}$ photon absorption rate for these SiO_2 -coated silicon grains is $\gamma_{\text{Si}} \approx 1.92 \times 10^{-6}(\chi/2000) \text{ s}^{-1} \text{ Si}^{-1}$, with $\langle h\nu \rangle_{\text{abs}} \approx 8.8\text{eV}$. The ERE emissivity per H is then $\langle h\nu \rangle_{\text{ERE}} \gamma_{\text{Si}} \eta_{\text{PL}} Z_{\text{Si}} / 4\pi \approx 4.40 \times 10^{-19} \eta_{\text{PL}} Z_{\text{Si}} \text{ erg s}^{-1} \text{ sr}^{-1} \text{ H}^{-1}$. From eq. (3) we thus require $\eta_{\text{PL}} Z_{\text{Si}} \approx 7.94 \times 10^{-8} 10^{0.4A_{0.68\mu\text{m}}}$.

Since $Z_{\text{Si}} \lesssim 0.75\text{ppm}$ the *observed* ERE intensity in NGC 2023 (eq.[3]) requires a photon conversion efficiency $\eta_{\text{PL}} \gtrsim 0.11 \times 10^{0.4A_{0.68\mu\text{m}}}$ if due to Si core- SiO_2 mantle nanoparticles.

4. Discussion

Si/SiO_2 core-mantle grains are heated primarily by absorption by the Si core (the photoluminescence of which is responsible for the ERE), since the SiO_2 mantle is almost nonabsorptive for $0.12 \lesssim \lambda \lesssim 4\mu\text{m}$; the core-mantle grains are cooled primarily by the SiO_2 mantle, since m'' is so small for Si in the infrared (see Figure 1). Therefore, increasing the amount of SiO_2 present (while holding the pure Si cores constant) will lead to only small changes in the IR emission resulting from the slight decrease in average grain temperature. The limits on η_{PL} will be only slightly affected by increasing the thickness of the SiO_2 mantles.

In §3 the grains are modelled as spherical. To investigate the sensitivity to shape variations, we have also calculated the IR emission spectra for grains with a sphere-peaked distribution of

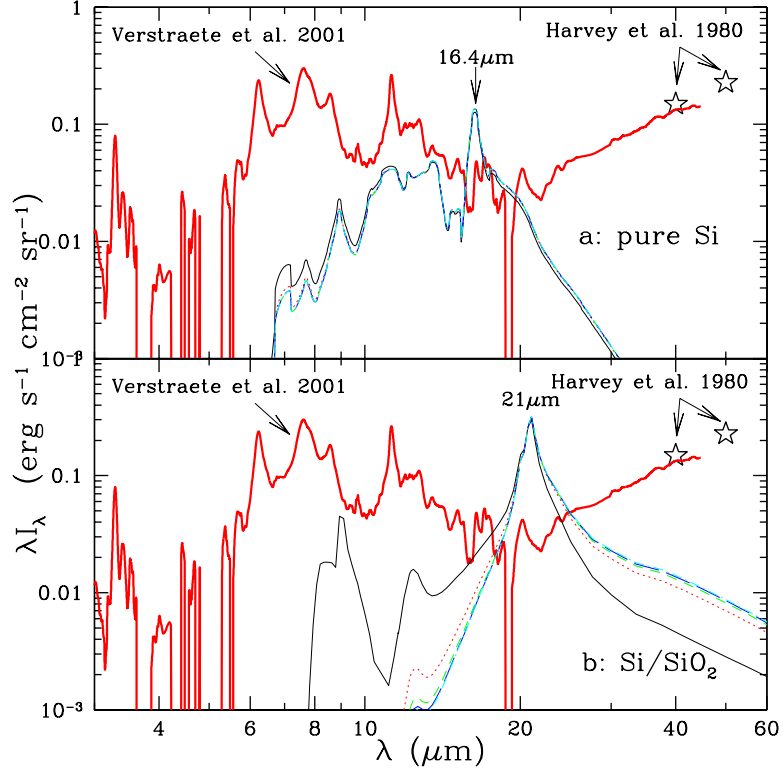


Fig. 3.— IR emission spectra of NGC 2023 (60'' S of HD 37903). The ISO SWS 2.4–45 μm spectrum (Verstraete et al. 2001) is plotted as heavy solid line. The KAO data (Harvey et al. 1980) is plotted as stars. Upper panel (a) – thin lines are model spectra calculated from *pure silicon* grains of $a = 10, 20, 30, 40, 50\text{\AA}$. For all sizes, Z_{Si} is fixed at 3ppm (i.e. $\text{Si}/\text{H}=3 \times 10^{-6}$). Note that the spectra for $a = 20, 30, 40, 50\text{\AA}$ are indistinguishable. Lower panel (b) – thin lines are model spectra calculated from *silicon core-SiO₂ mantle* grains with silicon core sizes of $a_{\text{Si}} = 10, 20, 30, 40, 50\text{\AA}$ (solid: 10 \AA ; dotted: 20 \AA ; dashed: 30, 40, 50 \AA). The spectra for $a_{\text{Si}} = 30, 40, 50\text{\AA}$ are indistinguishable). All grains have $Z_{\text{Si}}=6\text{ppm}$.

spheroidal shapes with $dP/dL_{\parallel} = 12L_{\parallel}[1 - L_{\parallel}]^2$ (Ossenkopf, Henning, & Mathis 1992) where L_{\parallel} is the so-called “depolarization factor” parallel to the grain symmetry axis (for spheres $L_{\parallel}=1/3$); this shape distribution peaks at spheres and drops to zero for the extreme cases $L_{\parallel} \rightarrow 0$ (infinitely thin needles) or $L_{\parallel} \rightarrow 1$ (infinitely flattened pancake). For core-mantle grains, we assume *confocal* geometry, with the above dP/dL_{\parallel} applying to the outer surface (the eccentricities and depolarization factors for the cores are different from those of the mantles – see Draine & Lee 1984). We find that the major change is the slight shift of the peak wavelength of the 21 μm Si-O feature: from 20.9 μm (spherical) to 21.0 μm ; the height of the feature is only reduced by $\approx 6\%$. We conclude that shape effects are minor.

The ERE surface brightness $\propto N_{\text{H}}\chi\eta_{\text{PL}}Z_{\text{Si}}/\cos\theta$. The IR surface brightness due to SNPs $\int I_{\nu}d\nu \propto N_{\text{H}}\chi Z_{\text{Si}}/\cos\theta$. While the relative strength of the 21 μm SiO₂ feature (or the 16 μm Si feature in the case of pure Si nanoparticles) depends on χ (through the grain temperature), this dependence is relatively weak for modest changes in χ . Therefore the observed ERE and

upper limits on the the $16\mu\text{m}$ and $21\mu\text{m}$ features allow us to obtain lower limits on η_{PL} which are independent of the values of N_{H} and the limb-brightening factor $1/\cos\theta$, and only weakly dependent on the value of χ .

One uncertainty in our analysis concerns the IR emission properties of nano-silicon crystals and nano- SiO_2 , which have not yet been experimentally investigated. In this work, our results are mainly based on the IR emissivities of bulk silicon and bulk SiO_2 . Nano-materials are expected to be more IR-active than their bulk counterparts (due to the symmetry-breaking surfaces) and therefore the detailed emission spectrum will be modified. However, the starlight energy absorbed by the grains has to be reradiated in the infrared, so the absence of detected spectral features implies upper limits on the SNP abundance.

The largest uncertainty in our analysis is the value of the foreground extinction A_{λ} required to “deredden” the ERE measurements. Unfortunately, A_{λ} has not been directly measured at the location where the ERE observations have been made. It would be extremely valuable to have ERE measurements made at a position where a reliable extinction has been determined – such as the emission bar $80''$ S of HD 39037 – or to have both IR and far-red observations of H_2 emission (allowing A_{λ} to be determined) at a location where the ERE has been measured.

5. Conclusions

As a test of the proposal that the observed ERE is due to crystalline silicon nanoparticles, we predict the infrared emission from such particles and compare it to the observed IR emission spectrum of NGC 2023. We consider both pure Si nanoparticles as well as pure Si cores with SiO_2 coatings. Since infrared features predicted for these particles are not observed, we obtain upper limits on the abundance of silicon nanoparticles in NGC 2023, thereby obtaining lower bounds on the photoluminescence efficiency η_{PL} if these particles are responsible for the ERE.

The final conclusion is dependent on the foreground extinction near $\lambda \approx 0.68\mu\text{m}$ where the ERE peaks. In §3.1 we argue that this extinction lies in the range $1.2 \lesssim A_{0.68\mu\text{m}} \lesssim 3.2$.

For pure Si nanoparticles, nondetection of an emission feature at $16.4\mu\text{m}$ implies $\eta_{\text{PL}} \gtrsim 0.055 \times 10^{0.4A_{0.68\mu\text{m}}}$. Thus for $A_{0.68\mu\text{m}} = 1.2$, pure Si nanoparticles could account for the observed ERE in NGC 2023 provided $\eta_{\text{PL}} \gtrsim 17\%$, but if $A_{0.68\mu\text{m}} = 3.2$, pure Si nanoparticles would have to have $\eta_{\text{PL}} \gtrsim 100\%$ to account for the ERE. While such a high value $\eta_{\text{PL}} \approx 100\%$ cannot be excluded for a silicon nanoparticle in vacuo, in the laboratory high photoluminescence efficiencies are seen only when the Si surfaces are “passivated” by an oxide coating.

An oxide coating, however, will cause the optically-active IR modes of SiO_2 to appear in the emission spectrum resulting in a strong emission feature at $21\mu\text{m}$ which has not been detected. For Si/ SiO_2 nanoparticles to explain the ERE, nondetection of the $21\mu\text{m}$ feature implies that the luminescence efficiency must be large: $\eta_{\text{PL}} \gtrsim 0.11 \times 10^{0.4A_{0.68\mu\text{m}}}$. Photoluminescence efficiencies

as high as 50% have been reported for Si/SiO₂ nanoparticles (Wilson, Szajowski, & Brus 1993), and in principle η_{PL} could approach 100%. However, if $A_{0.68\mu m} \gtrsim 2.7$, the ERE cannot be due to Si/SiO₂ nanoparticles since the required efficiency would then exceed 100%.

We have seen that spectrophotometry of both the ERE and the 15–25 μm emission spectrum, together with knowledge of the foreground extinction A_λ , can provide a strong test off the hypothesis that the ERE is due to silicon nanoparticles by constraining the required photoluminescence efficiency η_{PL} . Application of this test to NGC 2023 is at present inconclusive because of relatively large uncertainties concerning the foreground extinction $A_{0.68\mu m}$ in the red. The foreground extinction can, in fact, be determined by observations of K band ($\Delta v = -1$) and far-red ($\Delta v = -3$ and -4) emission lines originating from vibrational levels $v \geq 3$ of ultraviolet-pumped H₂ (McCartney et al. 1999).

Conclusive application of the test developed in this paper will be possible when the H₂ emission spectrum (both K band and far-red), 15–25 μm dust emission spectrum, and ERE intensity are measured at a common location in NGC 2023 or another suitable reflection nebula. Detection of the 16 μm or 21 μm emission feature would provide support for the silicon nanoparticle hypothesis, as well as providing a value for the photoluminescence efficiency η_{PL} . Failure to detect the 16 μm or 21 μm emission features (as is the case thus far in NGC 2023) provides lower limits on η_{PL} ; if these lower limits exceed 100%, the silicon nanoparticle hypothesis would be ruled out as the explanation for the ERE.

We especially thank L. Verstraete for providing us with the ISO spectrum of NGC 2023 prior to publication. We also thank S. Adachi, N. Koshida, and V.G. Zubko for sending us their optical constants of bulk silicon and nano-silicon; S. Adachi, L.J. Allamandola, J.M. Greenberg, Th. Henning, and K. Sellgren for helpful suggestions; and R.H. Lupton for the availability of the SM plotting package. This research was supported in part by NASA grant NAG5-7030 and NSF grants AST-9619429 and AST-9988126.

REFERENCES

Adachi, S. 1999, Optical Constants of Crystalline and Amorphous Semiconductors – Numerical Data and Graphical Information (Dordrecht: Kluwer)

Bohren, C.F., & Huffman, D.R. 1983, Absorption and Scattering of Light by Small Particles (New York: Wiley)

Cardelli, J.A., Clayton, G.C., & Mathis, J.S. 1989, ApJ, 345, 245

Draine, B.T., & Bertoldi, F. 1996, ApJ, 468, 269

Draine, B.T., & Bertoldi, F. 2000, in H₂ in Space, ed. F. Combes, & G. Pineau des Forêts (Cambridge University Press), in press

Draine, B.T., & Lee, H.M. 1984, *ApJ*, 285, 89

Draine, B.T., & Li, A. 2001, *ApJ*, 550, 000 (astro-ph/0011318)

Duley, W.W. 1985, *MNRAS*, 215, 259

Gordon, K.D., Witt, A.N., & Friedmann, B.C. 1998, *ApJ*, 498, 522

Gordon, K.D., Witt, A.N., Rudy, R.J., et al. 2000, *ApJ*, 544, 859

Gray, D.E. 1972, American Institute of Physics Handbook (McGraw-Hill Book Company)

Greenberg, J.M. 1968, in Stars and Stellar Systems, Vol. VII, ed. B.M. Middlehurst & L.H. Aller (Chicago: Univ. of Chicago Press), 221

Habing, H.J. 1968, *Bull. Astron. Inst. Netherlands*, 19, 421

Harrington, J.A., Rudisill, J.E., & Braunstein, M. 1978, *Appl. Opt.*, 17, 1541

Harvey, P.M., Thronson, H.A., Jr., & Gatley, I. 1980, *ApJ*, 235, 89

d'Hendecourt, L.B., Léger, A., Olofson, G., & Schmidt, W. 1986, *A&A*, 170, 91

Hofmeister, A.M., Rosen, L.J., & Speck, A.K. 2000, in Thermal Emission Spectroscopy and Analysis of Dust, Disks, and Regoliths, ed. M.L. Sitko, A.L. Sprague, & D.K. Lynch, ASP Conf. Series, 196, 291

Johnson, F.A. 1959, *Proc. Phys. Soc. London*, 73, 265

Koshida, N., Koyama, H., Suda, Y. et al. 1993, *Appl. Phys. Lett.*, 63, 2774

Ledoux, G., Ehbrecht, M., Guillois, O., et al. 1998, *A&A*, 333, L39

Li, A., & Draine, B.T. 2001, submitted to *ApJ* (astro-ph/0011319)

McCartney, M.S.K., Brand, P.W.J.L., Burton, M.G., & Chrysostomou, A. 1999, *MNRAS*, 307, 315

Ossenkopf, V., Henning, Th., & Mathis, J.S. 1992, *A&A*, 261, 567

Palik, E.D. 1991, Handbook of Optical Constants of Solids (Boston: Academic)

Papoulias, R., Conard, J., Guillois, O., et al. 1996, *A&A*, 315, 222

Sakata, A., Wada, S., Narisawa, T., et al. 1992, *ApJ*, 393, L83

Schmidt, G.D., Cohen, M., & Margon, B. 1980, *ApJ*, 239, L133

Seahra, S.S., & Duley, W.W. 1999, *ApJ*, 520, 719

Szomoru, A., & Guhathakurta, P. 1998, *ApJ*, 494, L93

Verstraete, L., Pech, C., Moutou, C., Sellgren, K., Wright, C.M., Giard, M., Léger, A., Timmermann, R., & Drapatz, S. 2001, A&A, accepted

Webster, A. 1993, MNRAS, 264, L1

Wilson, W.L., Szajowski, P.F., & Brus, L.E. 1993, Science, 262, 1242

Witt, A.N., & Boroson, T.A. 1990, ApJ, 355, 182

Witt, A.N., Gordon, K.D., & Furton, D.G. 1998, ApJ, 501, L111

Witt, A.N., & Malin, D.F. 1989, ApJ, 347, L25

Witt, A.N., & Schild, R. 1988, ApJ, 325, 837

Zubko, V.G., Smith, T.L., & Witt, A.N. 1999, ApJ, 511, L57